nature immunology

Autophagy is essential for effector CD8+ T cell survival and memory formation

Xiaojin Xu[1,5], Koichi Araki[1,5], Shuzhao Li[2], Jin-Hwan Han[1], Lilin Ye[1], Wendy G Tan[1], Bogumila T Konieczny[1], Monique W Bruinsma[3], Jennifer Martinez[4], Erika L Pearce[3], Douglas R Green[4], Dean P Jones[2], Herbert W Virgin[3] & Rafi Ahmed[1]

The importance of autophagy in the generation of memory CD8+ T cells *in vivo* is not well defined. We report here that autophagy was dynamically regulated in virus-specific CD8+ T cells during acute infection of mice with lymphocytic choriomeningitis virus. In contrast to the current paradigm, autophagy decreased in activated proliferating effector CD8+ T cells and was then upregulated when the cells stopped dividing just before the contraction phase. Consistent with those findings, deletion of the gene encoding either of the autophagy-related molecules Atg5 or Atg7 had little to no effect on the proliferation and function of effector cells, but these autophagy-deficient effector cells had survival defects that resulted in compromised formation of memory T cells. Our studies define when autophagy is needed during effector and memory differentiation and warrant reexamination of the relationship between T cell activation and autophagy.

CD8+ T cells provide protection against intracellular bacterial, parasitic and viral infections, as well as cancers[1,2]. Following stimulation with antigens, naive CD8+ T cells go through many rounds of proliferation, giving rise to effector T cells, which eliminate infected cells. Upon clearance of the antigens, most effector CD8+ T cells undergo apoptosis, leaving only a small pool of cells to survive and differentiate into memory cells[3–5]. During this naive-to-effector to memory-differentiation process, T cells undergo cellular and metabolic reprogramming to shift from anabolic processes and proliferation to catabolic processes and contraction of cell populations to generate memory. It is important to define the role of macroautophagy (called 'autophagy' here) during this process.

Autophagy is an evolutionarily conserved process that involves the engulfment and delivery of cytosolic contents to the lysosome for degradation[6–10]. This catabolic activity of autophagy is essential for cellular homeostasis and has been suggested to be inversely correlated with cell growth and proliferation[11]. In contrast to that paradigm, it has been reported that autophagy is upregulated in proliferating T cells[9,12,13]. Stimulation via the T cell antigen receptor (TCR) promotes the activation and proliferation of T cells and also induces signaling via the metabolic checkpoint kinase mTOR, which would be expected to inhibit rather than induce autophagy[8]. Thus, questions remain about why and how proliferating T cells upregulate autophagy in the presence of positive mTOR signaling when cells need more proteins and organelles to donate to daughter cells. Furthermore, because autophagy has been studied mainly *in vitro* during the activation of T cells after stimulation via the TCR, little is known about *in vivo* autophagy activity in antigen-specific T cells during the course of the differentiation of effector and memory T cells after viral infection.

The *in vivo* function of autophagy in antigen-specific T cells during viral infection remains unclear but is important, as pharmacological manipulation of autophagy is being considered as a treatment for many human diseases[14]. Mice with a conditional null mutation resulting in selective deletion of the gene encoding either of the autophagy-related molecules Atg5 or Atg7 during early T cell development (through the use of Cre recombinase expressed from T cell–specific gene *Lck*) have fewer mature peripheral T cells than their wild-type counterparts have[10,15]. Similarly, chimeric mice reconstituted with *Atg5*$^{-/-}$ fetal liver cells have fewer peripheral T cells than do chimeric mice reconstituted with wild-type fetal liver cells[9]. That study also showed that *Atg5*-deficient T cells exhibit diminished proliferative capacity following *in vitro* stimulation via the TCR[9]. Although such data indicate that autophagy has a key role in the development and homeostasis of T cells, they shed less light on the function of autophagy molecules in T cells responding to antigen because the cells studied had developed in the absence of autophagy molecules such as Atg5 or Atg7 and exhibited abnormalities in gene expression and mitochondrial number and function[10,15]. Thus, a new approach using phenotypically normal naive T cells is needed to study the function of autophagy during T cell activation *in vivo*.

Here we investigated two issues: the kinetics of autophagy activity, and the role of autophagy during the response to lymphocytic

[1]Emory Vaccine Center and Department of Microbiology and Immunology, Emory University School of Medicine, Atlanta, Georgia, USA. [2]Division of Pulmonary, Allergy and Critical Care Medicine, Department of Medicine, Emory University School of Medicine, Atlanta, Georgia, USA. [3]Department of Pathology and Immunology, Washington University School of Medicine, St. Louis, Missouri, USA. [4]Department of Immunology, St. Jude Children's Research Hospital, Memphis, Tennessee, USA. [5]These authors contributed equally to this work. Correspondence should be addressed to R.A. (rahmed@emory.edu), H.W.V. (virgin@wustl.edu) or K.A. (karaki@emory.edu).

Received 26 August; accepted 2 October; published online 2 November 2014; doi:10.1038/ni.3025

choriomeningitis virus (LCMV). In contrast to published observations, we found that autophagy was inversely correlated to T cell proliferation and was substantially inhibited during the early effector stage (that is, when the cells were highly proliferative). Autophagy activity was then upregulated at the peak of expansion (that is, when antigen was cleared and antigen-specific T cells were about to undergo the contraction phase). We also established the importance of autophagy-related proteins for the development of $CD8^+$ T cell memory *in vivo* by null mutation of the gene encoding either of two molecules essential for autophagy, Atg5 or Atg7, through the use of the granzyme B–Cre system, in which normal naive T cells developed and the genes encoding autophagy-related molecules were deleted only after T cells were activated with antigen. Our study provides insight into the kinetics and the function of autophagy in antigen-specific $CD8^+$ T cells during effector and memory differentiation.

RESULTS

Dynamic regulation of autophagy in virus-specific T cells

During an acute viral infection, naive $CD8^+$ T cells underwent vigorous clonal expansion, followed by contraction, in which a small percentage of effector cells survived to establish memory (**Fig. 1a**). To study autophagy in antigen-specific $CD8^+$ T cells through the distinct phases of the T cell response, we took several different approaches to analyze the autophagy pathway and autophagic flux in antigen-specific $CD8^+$ T cells after acute infection with the Armstrong strain of LCMV. We isolated P14 $CD8^+$ T cells, which have transgenic expression of a TCR specific for the LCMV glycoprotein peptide epitope of amino acids 33–41 (gp33), at distinct stages of the T cell response: the expansion phase (cells with a blasting phenotype; day 5 after infection, when virus-specific effector $CD8^+$ T cells are actively proliferating); the peak of expansion (day 8 after infection, when effector $CD8^+$ T cells stop proliferating and decrease in size); the contraction phase (day 15 after infection); and the memory phase (day 30 after infection) (**Fig. 1a**,**b**). To assess autophagy activity, we first measured the abundance of the microtubule-associated proteins LC3b-I and LC3b-II in the sorted P14 cells. LC3b-II, the lipidated form of LC3b-I, is a classic marker of autophagosomes and is incorporated into the elongating membrane that eventually forms the autophagosome and is subsequently degraded after delivery to the lysosome[7] (**Supplementary Fig. 1a**). The quantity of both LC3b-I and LC3b-II in antigen-specific $CD8^+$ T cells peaked at day 5 after infection (**Fig. 1c**). The accumulation of LC3b proteins in P14 cells without an increase in LC3b-encoding transcripts at day 5 after infection (**Supplementary Fig. 1b**) would be consistent with either induction of autophagy and increased production of these proteins or inhibition of lysosomal degradation of these proteins. To further assess autophagy activity, we therefore examined expression of the ubiquitin-binding scaffold protein p62 (sequestosome-1). p62 is a widely used marker for measuring autophagic activity, as it is both a substrate of autophagy and an adaptor in targeting ubiquitinated proteins for lysosomal degradation via the autophagy pathway[16] (**Supplementary Fig. 1a**). Similar to LC3b, p62 showed its greatest accumulation at day 5 after infection, which was not associated with an increase in the corresponding mRNA encoding p62 (**Fig. 1c** and **Supplementary Fig. 1c**). We also investigated whether LC3b and p62 proteins accumulated at a much earlier stage of T cell activation. In these experiments, we injected the LCMV gp33 peptide noted above into P14 mice to activate all P14 cells in a short, synchronized time frame. Similar to the results obtained for the activated P14 cells collected from day 5 after infection, we detected more LC3b and p62 proteins at 20 h after activation without an increase in their mRNA (**Supplementary Fig. 1d**,**e**). These data suggested an altered flux in the autophagy pathway at the early effector stage of the T cell response and were most consistent with a reduction in autophagy during antigen-driven activation of T cells *in vivo*.

To further define how the highly dynamic autophagy pathway is regulated *in vivo* during the $CD8^+$ T cell response, we generated a reporter system for autophagy activity by fusing a recombinant mouse LC3b protein to green fluorescent protein (GFP)[7] (**Fig. 2a**). We introduced this fusion protein into P14 cells with a retroviral vector system (consisting of mouse stem cell virus (MSCV) with expression of the transduction marker Thy-1.1 under control of an internal ribosomal entry site (MIT)), by which P14 cells transduced with MIT could be distinguished by the expression of Thy-1.1 (**Fig. 2a** and **Supplementary Fig. 2a**). This reporter system allowed us to quantify autophagy activity at varying times following LCMV infection by measuring GFP expression by flow cytometry; high autophagy activity was reflected by a reduction in GFP intensity due to either the enhanced degradation of GFP-LC3b protein through the autophagy pathway or fluorescence quenching of GFP by low pH after fusion of autophagosomes with lysosomes[17]. As a control we used a GFP-tagged mutant of LC3b with substitution of alanine for the glycine at position 120 (G120A), which results in removal of the carboxy-terminal amino acid to which phosphatidylethanolamine is conjugated during the generation of LC3b-II from LC3b-I (**Fig. 2a**); this results in a failure of this molecule to be incorporated into autophagosomes. Consistent with our immunoblot analysis of LC3b and p62, at day 5 after infection, the GFP intensity of wild-type and mutant LC3b was similar (**Fig. 2b**), indicative of lower autophagic flux. We also observed similar amounts of GFP intensity for wild-type and mutant LC3b at much earlier times after infection (days 2 and 3; **Supplementary Fig. 2b**–**e**). However, at day 8 after infection, there was a difference between wild-type LC3b and mutant LC3b, and we saw a greater frequency of GFP^- P14 cells transduced with retrovirus encoding wild-type LC3b than of those transduced with retrovirus encoding the G120A mutant (**Fig. 2b**,**c**), which suggested substantially greater flux through the autophagy pathway at day 8 than at day 5. This difference between wild-type LC3b and mutant LC3b in their GFP intensity remained through day 30 after infection (**Fig. 2b**,**c**).

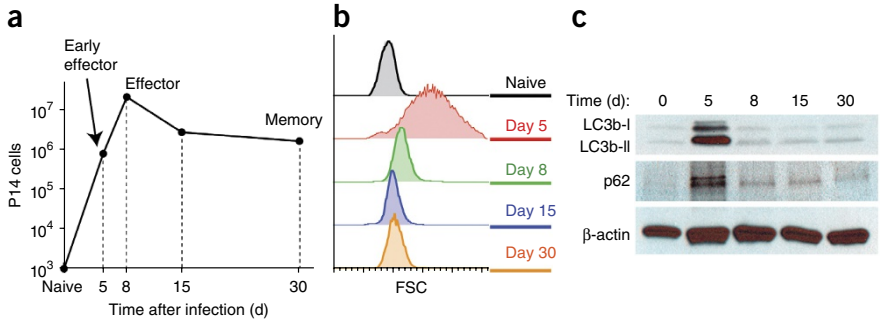

Figure 1 Analysis of autophagy in virus-specific $CD8^+$ T cells during a viral infection. (**a**) Kinetics of the appearance of P14 cells in spleens of C57BL/6 mice given adoptive transfer of 1×10^4 P14 cells, monitored after infection of recipients with LCMV Armstrong strain. (**b**) Flow cytometry of cell size at various stages of P14 differentiation, assessed by forward scatter (FSC). (**c**) Immunoblot analysis of LC3b and p62 at various stages of P14 differentiation. Data are representative of two independent experiments with samples pooled from 5–20 mice for each time point.

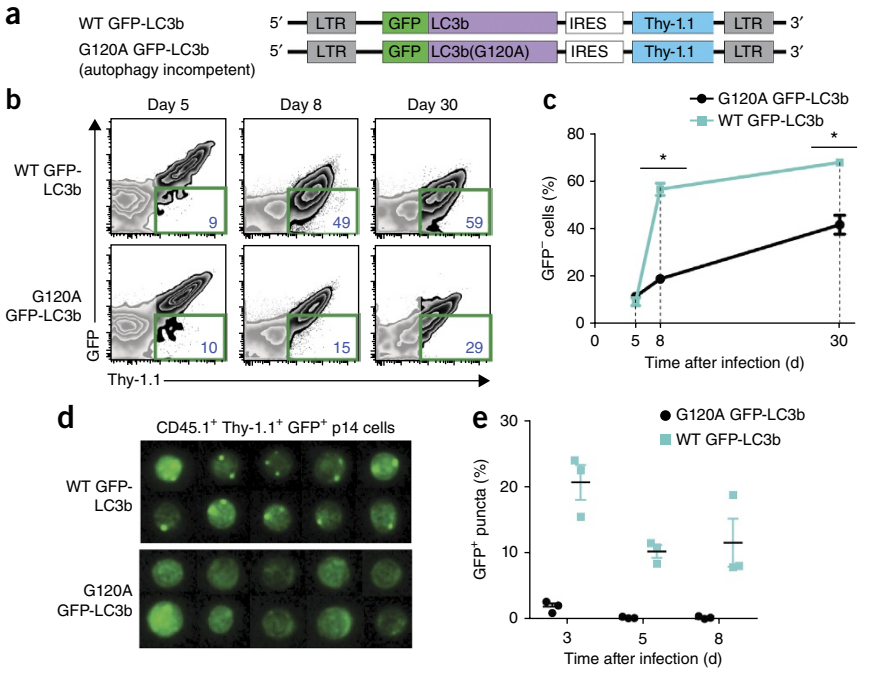

Figure 2 Autophagic flux in virus-specific CD8⁺ T cells is inversely correlated with cell proliferation status. (**a**) MSCV retroviral constructs introduced in P14 cells (**Supplementary Fig. 2a**) to probe for autophagy activity, showing the transgenes encoding GFP-tagged wild-type LC3b (top; WT GFP-LC3b) and the GFP-tagged G120A mutant of LC3b (bottom; G120A GFP-LC3b). LTR, long terminal repeat; IRES, internal ribosomal entry site. (**b**) Flow cytometry of P14 cells from the spleens of recipient mice given adoptive transfer of P14 cells transduced with retrovirus as in **a**, assessed on days 5, 8 and 30 after infection of recipients with LCMV. Numbers in blue outlined areas indicate percent GFP⁻ cells among transduced (Thy-1.1⁺) P14 cells. (**c**) Summary of results in **b**, showing autophagy activity as percent GFP⁻ cells. *$P \leq 0.0005$ (unpaired *t*-test). (**d**) Multispectral-imaging flow cytometry of P14 cells from mice treated as in **b**, assessed on day 8 after infection, showing GFP signals from GFP⁺ transduced (CD45.1⁺ Thy-1.1⁺) P14 cells. Original magnification, ×60. (**e**) Summary of results in **d**, presented as the frequency of cells with more than one GFP⁺ punctum among vector transduced Thy-1.1⁺ P14 cells. Each symbol represents an individual mouse; small horizontal lines indicate the mean (±s.e.m.). Data are representative of three independent experiments (**b**,**d**) or three independent experiments with three or more mice per group (**e**; error bars, s.e.m.) or six mice per group (**c**; error bars, s.e.m.).

In addition to results obtained with this P14 system, we saw a similar change in autophagy flux in endogenous CD8⁺ T cells specific for the LCMV gp33 epitope (**Supplementary Fig. 3**). To apply the reporter system to endogenous cells, we transduced hematopoietic stem cells with MIT containing sequence encoding GFP-tagged wild-type LC3b or G120A mutant LC3b, followed by adoptive transfer of the transduced cells into lethally irradiated mice (**Supplementary Fig. 3a**). After reconstitution, we infected mice with the Armstrong strain of LCMV and monitored GFP expression in MIT-transduced CD8⁺ T cells positive for a tetramer of H-2D^b and the LCMV gp33 epitope (H-2D^b–gp33) (**Supplementary Fig. 3a**). Similar to the results obtained for P14 T cells, GFP expression in H-2D^b–gp33⁺ cells transduced with MIT carrying sequence encoding wild-type LC3b was similar to that in cells transduced with MIT carrying sequence encoding the G120A mutant at day 6 after infection, and we observed a substantial decrease in the expression of GFP-tagged wild-type LC3b at days 8, 15 and 30 after infection (**Supplementary Fig. 3b**). These data indicated that autophagy was diminished in antigen-specific CD8⁺ T cells during the clonal expansion phase but was substantially increased following the expansion phase and into the memory phase.

As an additional assessment of autophagy, we visualized GFP-LC3b puncta by multispectral imaging flow cytometry (ImageStream) to quantify autophagosomes; GFP puncta reflected the incorporation of lipidated GFP-LC3b onto the elongating phagophore membrane that subsequently formed the autophagosomes. On days 3, 5 and 8 after infection, we observed puncta in P14 cells transduced to express GFP-taggd wild-type LC3b, although we detected a slightly higher frequency of puncta on day 3 after infection (**Fig. 2d**,**e**). These data indicated that antigen-specific CD8⁺ T cells were able to form autophagosomes during the expansion phase of the T cell response. Our results suggested that the low autophagy activity during clonal expansion was due to diminished flux through the lysosomal degradation pathway and that, on conclusion of the clonal expansion phase (day 8 after infection), autophagic flux was much greater.

Our results for the *in vivo* kinetics of autophagy activity in virus-specific CD8⁺ T cells were unexpected, because published *in vitro* studies have shown that T cells increase autophagy after TCR stimulation[9,12,13]. To further confirm our findings and determine if autophagolysosome formation is indeed inhibited during the clonal expansion phase, we made retroviral vectors expressing a fusion of the red fluorescent protein mCherry and GFP-LC3b (**Fig. 3a**). mCherry has more stable fluorescence than that of GFP under acidic conditions, such as following the fusion of autophagosomes to lysosomes[7,18,19]; this allowed us to assess whether LC3b had been delivered from autophagosomes into acidic autophagolysosomes. With this system, enhanced autophagic flux results in less GFP fluorescence than mCherry fluorescence due to the delivery of LC3b into an acidic environment[7,18,19]. We assessed the formation of autophagolysosomes in antigen-specific CD8⁺ T cells during the T cell clonal-expansion phase (day 5) and at the peak of T cell responses (day 8; **Fig. 3b**). Consistent with our results reported above, proliferating effector CD8⁺ T cells at day 5 after infection were larger than effector CD8⁺ T cells at day 8 after infection, when these cells had stopped proliferating (**Fig. 3c**). The ratio of fluorescence intensity of GFP to that of mCherry in P14 cells transduced with retrovirus expressing wild-type LC3b was very similar to that in P14 cells transduced with retrovirus expressing G120A mutant LC3b at day 5 after infection (**Fig. 3d**,**e**), which indicated that autophagy decreased in proliferating virus-specific CD8⁺ T cells. In contrast, at day 8 after infection, GFP fluorescence was lower than mCherry fluorescence specifically in the cells transduced to express wild-type LC3b (**Fig. 3d**) and the ratio of fluorescence intensity (GFP/mCherry) was 4.3-fold lower in cells transduced to express wild-type LC3b than in cells transduced to express G120A LC3b (**Fig. 3e**). These results were consistent with increased delivery of LC3b into autophagolysosomes due to induction of autophagy between day 5 and day 8 after infection. Thus, autophagic flux was inhibited during the T cell clonal expansion phase through the impairment of autophagosome maturation into

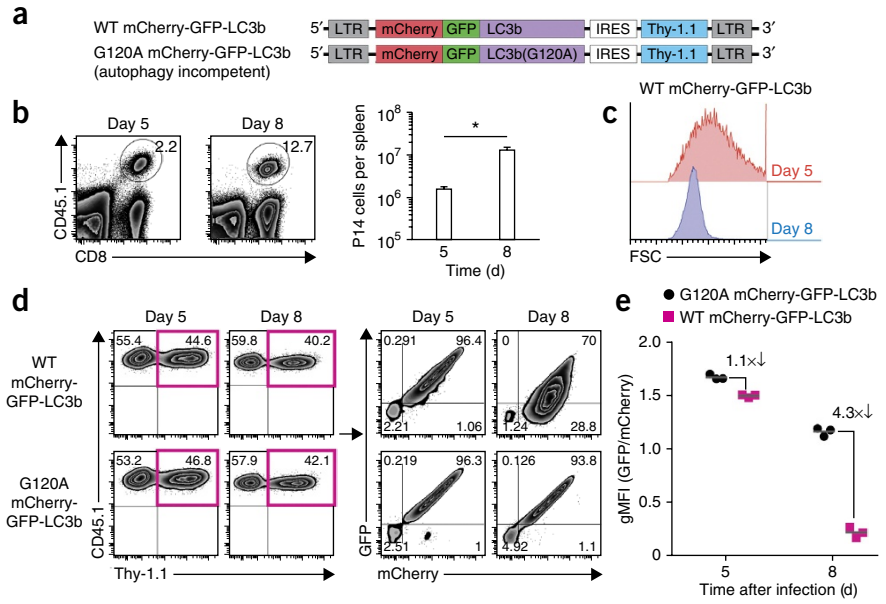

Figure 3 Autophagic flux is inhibited during the T cell clonal expansion phase via impairment of autophagosome maturation into autophagolysosomes. (**a**) mCherry-GFP-LC3b MSCV retroviral constructs (presented as in **Fig. 2a**) used for transduction of P14 cells (**Supplementary Fig. 2a**). (**b**) Flow cytometry of splenocytes from recipient mice ($n = 6$) given adoptive transfer of P14 cells transduced with retrovirus as in **a**, assessed on days 5 and 8 after infection of recipients with LCMV (left), and quantification of P14 cells per spleen (right). Numbers adjacent to outlined areas (left) indicate percent P14 (CD45.1$^+$) cells. *$P \leq 0.0005$ (unpaired *t*-test). (**c**) Flow cytometry of the size of P14 cells transduced with wild-type mCherry-GFP-LC3b retrovirus (assessed as in **Fig. 1b**) in mice treated as in **b**, assessed at days 5 and 8 after infection. (**d**) Efficiency of retroviral transduction (left) and expression of GFP and mCherry (right) in retrovirus-transduced P14 cells, assessed by flow cytometry gated on CD45.1$^+$ P14 cells (left) or CD45.1$^+$Thy-1.1$^+$ P14 cells (right). Numbers in quadrants indicate percent CD45.1$^+$Thy-1.1$^-$ (untransduced) P14 cells (top left) or CD45.1$^+$Thy-1.1$^+$ (transduced) P14 cells (top right; magenta) (left) or percent cells in each (right). (**e**) Ratio of the geometric mean fluorescence intensity (gMFI) of GFP to that of mCherry (GFP/mCherry) for the cells in **d**; each symbol represents an individual mouse; numbers above lines connecting groups indicate difference in ratio. Data are representative of two independent experiments with three or more mice per group (error bars (**b**), s.e.m.).

autophagolysosomes, followed by a rapid induction of autophagy concurrent with the peak of CD8$^+$ T cell effector responses at day 8 after infection.

Atg7 and Atg5 are critical for CD8$^+$ T cell memory generation

To determine the importance of the increase in autophagy activity during the transition phase from effector CD8$^+$ T cells to memory CD8$^+$ T cells, we generated mice with a conditional null mutation by crossing mice with *lox*P-flanked *Atg7* alleles (*Atg7*$^{fl/fl}$) or *Atg5* alleles (*Atg5*$^{fl/fl}$) with mice carrying a transgene encoding Cre driven by the promoter of the gene encoding granzyme B (*Gzmb*-Cre)[20–22] to generate *Atg7*$^{fl/fl}$*Gzmb*-Cre or *Atg5*$^{fl/fl}$*Gzmb*-Cre mice. In this system, deletion of *Atg7*$^{fl/fl}$ or *Atg5*$^{fl/fl}$ occurs specifically upon the expression of *Gzmb* in activated CD8$^+$ T cells.

We infected *Atg7*$^{fl/fl}$*Gzmb*-Cre mice with LCMV Armstrong strain. To establish the efficacy of the *Gzmb*-Cre system in the context of *Atg7*$^{fl/fl}$*Gzmb*-Cre mice, we isolated H-2D^b–gp33$^+$ CD8 T cells 8 d after infection (**Supplementary Fig. 4a**). Assessment of gene deletion by quantitative PCR showed a reduction of more than 20-fold in genomic copies of the *Atg7*^{fl} allele in H-2D^b–gp33-specific CD8$^+$ T cells, indicative of 95% deletion of the *Atg7*^{fl} allele (**Fig. 4a**). We noted similar deletion of *Atg7*^{fl} in the bulk-activated (CD44^{hi}CD62L^{lo}) CD8$^+$ T cell population, >95% of which were LCMV specific and expressed granzyme B at day 8 after infection[23] (**Fig. 4a** and **Supplementary Fig. 4b**). The extent of *Atg7*^{fl} deletion was also reflected by the abundance of Atg7 protein in bulk-activated CD8$^+$ T cells, whereby Atg7 protein was barely discernible in the CD44^{hi}CD62L^{lo} effector CD8$^+$ T cell population from *Atg7*$^{fl/fl}$*Gzmb*-Cre mice (**Fig. 4b**). We also confirmed the absence of Atg7 protein by assessing its catalytic activity. Atg7 catalyzes reactions that result in Atg5-Atg12 conjugation and lipidation of LC3-I to give rise to LC3b-II (ref. 6). The enzymatic activity of Atg7 in the effector CD8$^+$ T cells was significantly diminished, as indicated by the absence of both Atg5-Atg12 conjugation and lipidated LC3-II (**Fig. 4b**). Instead, we detected an abundance of Atg5 protein as an unconjugated species (**Fig. 4b**). Furthermore, p62 accumulated in the absence of Atg7 (**Fig. 4b**), indicative of defects in autophagic activity. These data indicated the high efficacy of the Cre-*lox*P system in deleting the target *Atg7*^{fl} allele from LCMV-specific CD8$^+$ T cells and the consequent loss of autophagy at a time point (day 8) at which autophagy would normally be increased. In addition, these data confirmed the results of the assays of LC3b and p62 used to measure autophagic flux in primary T cells *in vivo*.

To assess the importance of Atg7 in antigen-specific CD8$^+$ T cells, we infected *Atg7*$^{fl/fl}$*Gzmb*-Cre mice with LCMV Armstrong strain and monitored the differentiation of LCMV-specific CD8$^+$ T cells over time. At 8 d after infection, H-2D^b–gp33$^+$ CD8$^+$ T cell populations had undergone considerable expansion in both *Atg7*$^{fl/fl}$ mice (which do not express Cre) and *Atg7*$^{fl/fl}$*Gzmb*-Cre mice (**Fig. 4c**). Also at day 8 after infection, the memory precursor population characterized as KLRG1^{lo}CD127^{hi} was present among *Atg7*-deficient H-2D^b–gp33-specific cells in a proportion similar to that among wild-type cells[3–5] (**Fig. 4c**). Other phenotypic markers, including CD44 and CD62L, showed no considerable difference between the two groups (**Supplementary Fig. 4c**). Despite a small reduction in the number of antigen-specific CD8$^+$ T cells among peripheral blood mononuclear cells at day 8 after infection (**Fig. 4c**), we detected antigen-specific CD8$^+$ T cells in similar quantities in all tissues examined, including spleen, liver and lungs, in the *Atg7*$^{fl/fl}$ and *Atg7*$^{fl/fl}$*Gzmb*-Cre mice (**Fig. 4d**). In support of those data, we did not observe any difference between wild-type and *Atg7*-deficient antigen-specific CD8$^+$ T cells in their proliferation (as measured by incorporation of the thymidine analog BrdU) or in the number of cells undergoing apoptosis at day 5 after infection, when T cells are rapidly proliferating (**Supplementary Fig. 4d–h**).

An important function of CD8$^+$ T cells is the ability to produce the antiviral cytokines interferon-γ (IFN-γ) and tumor-necrosis factor (TNF). *Ex vivo* stimulation of splenocytes at day 8 after infection using peptides indicated little difference in the ability of cells to produce these cytokines or number of cells producing them (**Fig. 4e**). In addition, we no longer detected virus in the serum, spleen, liver or

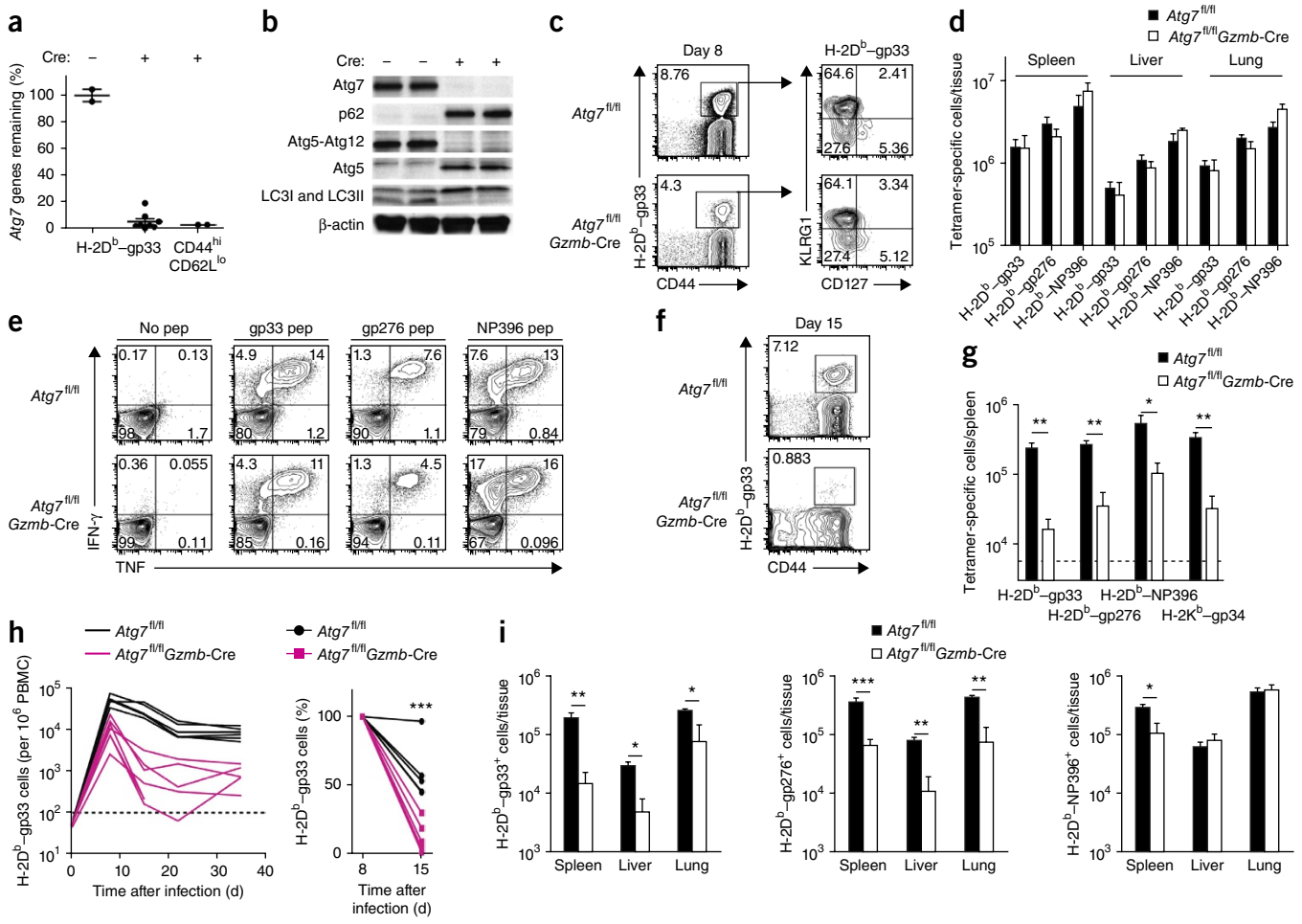

Figure 4 Atg7 deficiency results in survival defects in effector CD8$^+$ T cells during the effector-to-memory transition. (**a**) Genomic deletion of *Atg7* in H-2D^b–gp33$^+$ T cells and in total activated (CD44^{hi}CD62L^{lo}) CD8$^+$ T cells from *Atg7*$^{fl/fl}$ mice (Cre –) and *Atg7*$^{fl/fl}$*Gzmb*-Cre mice (Cre +) at day 8 after infection with LCMV Armstrong strain; results are presented relative to those of *Atg7*$^{fl/fl}$ mice, set as 100%. Each symbol represents an individual mouse; small horizontal lines indicate the mean (±s.e.m.). (**b**) Immunoblot analysis of Atg7 and the products of its enzymatic activity (left margin) in CD44^{hi}CD62L^{lo} CD8$^+$ T cells isolated at day 8 after infection as in **a**; β-actin serves as a loading control. (**c**) Flow cytometry of T cells in the peripheral blood at day 8 after infection as in **a**, gated on CD8$^+$ T cells (left), and of the H-2D^b–gp33$^+$ T cells identified at left, identifying terminal effector (KLRG1^{hi}CD127^{lo}) and memory precursor (KLRG1^{lo}CD127^{hi}) populations (right). Numbers adjacent to outlined areas (left) indicate percent H-2D^b–gp33$^+$ T cells; numbers in quadrants (right) indicate percent cells in each. (**d**) Total antigen-specific CD8$^+$ T cells in the spleen, liver and lungs at day 8 after infection as in **a**. (**e**) Production of IFN-γ and TNF in cells obtained 8 d after infection and stimulated *ex vivo* with various peptides (above plots), gated on total CD8$^+$ T cells. Numbers in quadrants indicate percent cells in each. (**f**) Flow cytometry of CD8$^+$ T cells in the peripheral blood of mice at day 15 after infection as in **a** (numbers in plots as in **c**, left). (**g**) Quantification of tetramer-positive cells in spleens at day 15 after infection as in **a**. (**h**) Kinetics of the appearance H-2D^b–gp33$^+$ CD8$^+$ T cells among peripheral blood mononuclear cells (PBMCs) after infection as in **a** (left); each line represents one mouse. Right, frequency of H-2D^b–gp33$^+$ CD8$^+$ T cells remaining on day 15 relative to that on day 8, set as 100%. (**i**) Quantification of tetramer-positive cells at day 30 after infection as in **a**. Horizontal dashed lines (**g**,**h**) indicate the limit of detection. $^*P \le 0.05$, $^{**}P \le 0.005$ and $^{***}P \le 0.0005$ (unpaired *t*-test). Data were pooled from two independent experiments (**a**) or at least two independent experiments (**c**–**i**) with three to seven mice per group (error bars, s.e.m.) or are from one experiment with samples obtained from two independent experiments (**b**).

lungs of *Atg7*$^{fl/fl}$ or *Atg7*$^{fl/fl}$*Gzmb*-Cre mice by day 8 after infection (data not shown). Our data demonstrated that virus-specific CD8$^+$ T cells deficient in *Atg7* were able to proliferate and differentiate into functional effector T cells that were similar to their wild-type counterparts. This was consistent with our finding that autophagy was actually diminished in proliferating virus-specific CD8$^+$ T cells.

Immediately following the peak of expansion, we observed the sharpest decrease in virus-specific CD8$^+$ T cells in *Atg7*-deficient cells between day 8 and day 15 after infection (**Fig. 4f–h**). T cells specific for tetramers containing the dominant LCMV epitopes in *Atg7*$^{fl/fl}$*Gzmb*-Cre mice, including H-2D^b–gp33, H-2D^b–gp276, H-2D^b–NP396 and H-2K^b–gp34, were approximately 5- to 10-fold less abundant in the spleens of *Atg7*$^{fl/fl}$*Gzmb*-Cre mice than in those of *Atg7*$^{fl/fl}$ mice (**Fig. 4g**). Few antigen-specific T cells survived the contraction phase to transition into the memory phase (day 30 after infection) in lymphoid or nonlymphoid tissues or in the peripheral blood (**Fig. 4h,i**). Overall, these data indicated that Atg7 was important for the survival of effector CD8$^+$ T cells and that a defective autophagy pathway compromised the formation of a functional CD8$^+$ T cell memory pool. These results correlated very closely with the *in vivo* kinetics of autophagy. Thus, the survival defects of autophagy-deficient effector T cells occurred after day 8 after infection, concurrent with enhanced autophagy of virus-specific T cells.

We sought to determine whether the ubiquitin-like conjugation systems necessary for autophagy were required for the formation of T cell memory by evaluating the importance of a second essential

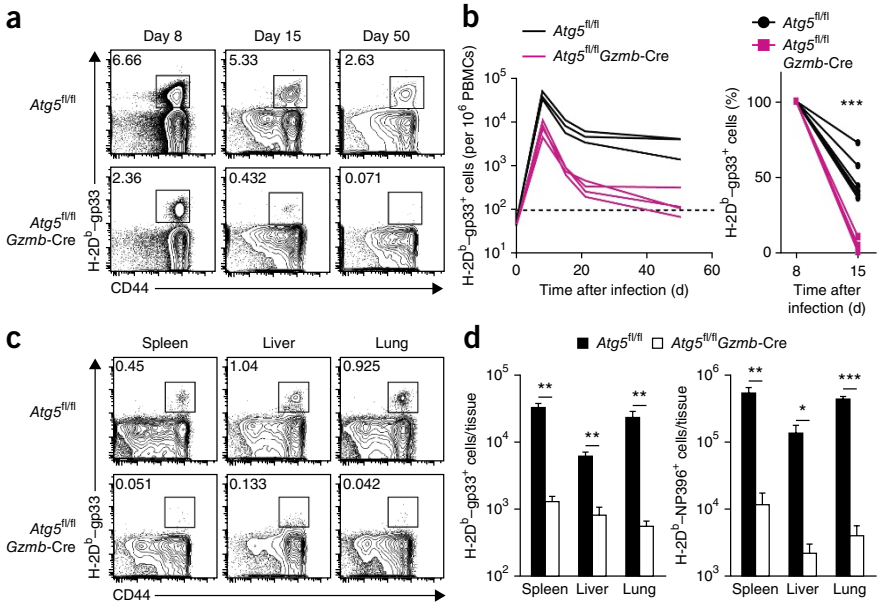

Figure 5 Survival defects of Atg5-deficient T cells during the contraction phase following infection with LCMV Armstrong strain. (**a**) Flow cytometry of circulating LCMV-specific CD8$^+$ T cells among peripheral blood mononuclear cells from *Atg5*$^{fl/fl}$ and *Atg5*$^{fl/fl}$*Gzmb*-Cre mice on days 8, 15 and 50 after infection with LCMV Armstrong strain. Numbers adjacent to outlined areas indicate percent H-2D^b–gp33$^+$ T cells, gated on CD8$^+$ T cells. (**b**) Longitudinal kinetics of the appearance of H-2D^b–gp33$^+$ T cells in the peripheral blood of mice as in **a** (left), and percent H-2D^b–gp33$^+$ CD8$^+$ T cells remaining on day 15 (right) (all presented as in **Fig. 4h**). (**c**) Flow cytometry of T cells in tissues on day 279 after infection as in **a** (numbers in plots as in **a**, among total gated CD8$^+$ T cells). (**d**) Total T cells specific for H-2D^b–gp33 (left) or H-2D^b–NP396 (right) in the spleen, liver and lungs of mice as in **a**. $^*P \le 0.05$, $^{**}P \le 0.005$ and $^{***}P \le 0.0005$ (unpaired *t*-test). Data are representative of two independent experiments with three to seven mice per group (error bars (**d**), s.e.m.).

autophagy-related protein, Atg5. Similar to the *Atg7*$^{fl/fl}$*Gzmb*-Cre phenotype, *Atg5*$^{fl/fl}$*Gzmb*-Cre mice infected with LCMV Armstrong strain demonstrated an initial expansion phase (day 8 after infection), followed by a substantial loss of antigen-specific CD8$^+$ T cells (**Fig. 5a**,**b**). We saw this loss in antigen-specific T cells in all tissues examined at the memory phase in the *Atg5*$^{fl/fl}$*Gzmb*-Cre mice (**Fig. 5c**,**d**). These data indicated a prosurvival role for proteins involved in the autophagy membrane-elongation complex in antigen-specific CD8$^+$ T cells.

The conditional null-mutation system is a powerful tool for investigating the function of a protein in a specific cell population. However, one caveat is that the substantial depletion of antigen-specific CD8$^+$ T cells observed in *Atg7*$^{fl/fl}$*Gzmb*-Cre mice and *Atg5*$^{fl/fl}$*Gzmb*-Cre mice during the course of LCMV infection (**Figs. 4** and **5**) might have an effect on host environmental factors, such as inflammatory cytokines that could compromise the survival and differentiation of T cells. Furthermore, other cell types, such as natural killer cells, also express granzyme B, which introduces an additional level of complexity in comparisons of experimental and control mice. Published work has linked natural killer cells to the modulation of T cell immunity[24,25]. To address these issues, we generated chimeras by reconstituting wild-type C57BL/6 (CD45.1$^+$) recipient mice with a mixture of congenitally marked bone marrow cells from wild-type C57BL/6 (CD45.1$^+$) donor mice and *Atg7*$^{fl/fl}$*Gzmb*-Cre (CD45.2$^+$) donor mice (**Supplementary Fig. 5a**). This system allowed us to compare changes in the number of wild-type and *Atg7*$^{fl/fl}$*Gzmb*-Cre antigen-specific CD8$^+$ T cells in the same environment (in the same mouse) and excluded the possibility of factors that act on only one population of these cells. As a control, we also generated chimeras by reconstituting wild-type recipient mice with a mixture of bone marrow from *Atg7*$^{fl/fl}$ (CD45.2$^+$) donor mice and wild-type (CD45.1$^+$) donor mice. After reconstitution, we challenged the recipient mice with LCMV Armstrong strain and assessed virus-specific CD8$^+$ T cells over time. At day 8 after infection, there was a substantial expansion of antigen-specific T cell populations from both *Atg7*$^{fl/fl}$ donor cells and *Atg7*$^{fl/fl}$ *Gzmb*-Cre donor cells (**Fig. 6a**,**b**). We longitudinally analyzed the responses of CD8$^+$ T cells specific for H-2D^b–gp33 or H-2D^b–NP396 during the effector and memory stages (**Fig. 6a**,**b** and **Supplementary Fig. 5c**). Similar to the results obtained for the mice with conditional null mutations, we observed a decrease of more than 90% in *Atg7*-deficient LCMV-specific CD8$^+$ T cells (CD45.2$^+$) from day 8 to day 15 in chimeras reconstituted with *Atg7*$^{fl/fl}$*Gzmb*-Cre bone marrow plus C57BL/6 bone marrow, compared with a moderate decrease of 50–60% in the corresponding wild-type (CD45.2$^+$) population in control chimeras reconstituted with *Atg7*$^{fl/fl}$ bone marrow plus C57BL/6 bone marrow (**Fig. 6a**,**b**). At 4 weeks after infection, there were almost no antigen-specific CD8$^+$ T cells of *Atg7*$^{fl/fl}$*Gzmb*-Cre (CD45.2$^+$) origin throughout the peripheral blood (**Fig. 6a**,**b**) and lymphoid and nonlymphoid tissues of chimeras reconstituted with *Atg7*$^{fl/fl}$*Gzmb*-Cre bone marrow plus C57BL/6 bone marrow (**Fig. 6c**). A considerable proportion of naive (CD44^{lo}) CD8$^+$ T cells from the *Atg7*$^{fl/fl}$*Gzmb*-Cre donor persisted in the chimeras (**Supplementary Fig. 5b**), which indicated specific loss of antigen-experienced effector CD8$^+$ T cells from *Atg7*$^{fl/fl}$*Gzmb*-Cre mice throughout the progression of infection. The cells of wild-type (CD45.1$^+$) origin made up most of the reconstituted population in the chimeras (**Supplementary Fig. 5b**), so the physiological and pathological conditions closely resembled those of the wild-type mice. Hence, in the absence of potential external variables, such as changes introduced in other cell types or any subtle variations in viral clearance, the defects rising from *Atg7* deficiency were cell-intrinsic properties that affected survival of the antigen-specific effector CD8$^+$ T cells to the memory phase. Thus, these data confirmed that the autophagy pathway was critical for memory T cell formation.

Distinct metabolic profiles of *Atg7*$^{-/-}$ effector T cells

To investigate the potential mechanism underlying the survival defects of the *Atg7*-deficient CD8$^+$ T cells, we performed metabolomic and transcriptomic analyses of antigen-specific T cells from *Atg7*-deficient (*Atg7*$^{fl/fl}$*Gzmb*-Cre) or 'wild-type' (*Atg7*$^{fl/fl}$) mice at 8 d after infection with LCMV Armstrong strain. We selected this time point as being representative of a transition point in T cell differentiation before substantial loss of *Atg7*-deficient cells had occurred. In the H-2D^b–gp33$^+$ CD8$^+$ T cells isolated from mice at 8 d after infection, the overall gene-expression pattern of the *Atg7*-deficient CD8$^+$ T cells closely resembled that of the 'wild-type' group; only a small number of genes showed a substantial difference in expression in the two groups in the DNA microarray data, mostly those encoding molecules associated with the cell cycle (data not shown). However, these cells exhibited distinct metabolic profiles, as measured on a

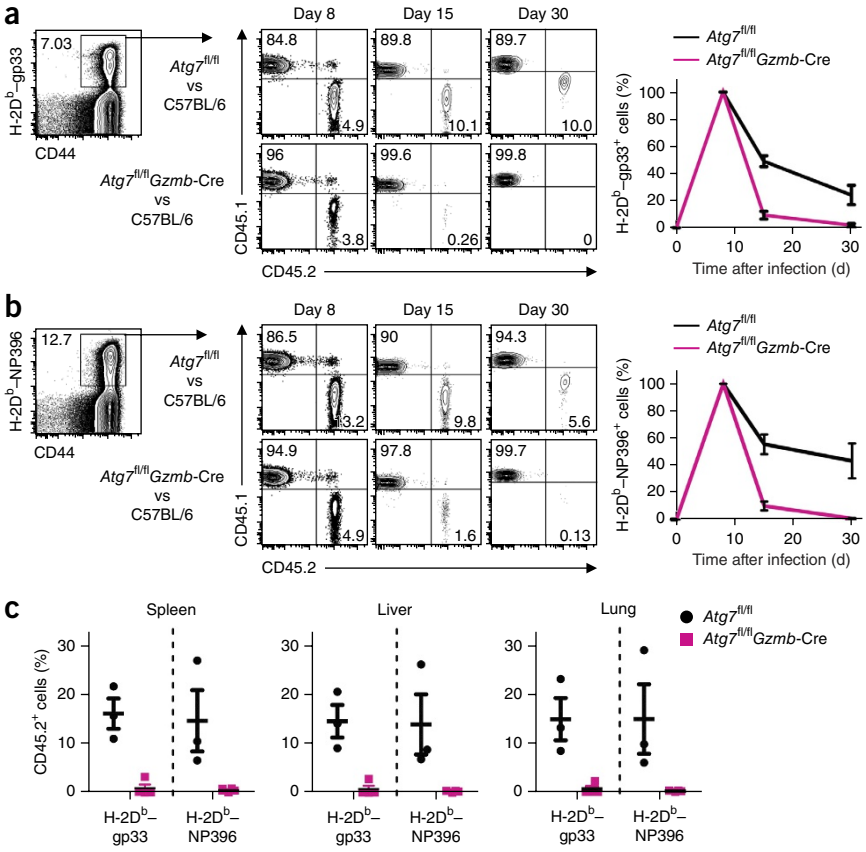

Figure 6 Antigen-specific CD8$^+$ T cells lacking *Atg7* exhibit cell-intrinsic defects in the development into long-term memory cells in chimeras. (**a**,**b**) Flow cytometry of CD8$^+$ T cell obtained from chimeras generated (as in **Supplementary Fig. 5a**) by reconstitution of wild-type mice with a mixture of bone marrow cells from *Atg7*$^{fl/fl}$ mice and wild-type C57BL/6 mice (*Atg7*$^{fl/fl}$ vs C57BL/6) or from *Atg7*$^{fl/fl}$*Gzmb*-Cre mice and wild-type C57BL/6 mice and (*Atg7*$^{fl/fl}$*Gzmb*-Cre vs C57BL/6), gated (far left) as populations specific for H-2D^b–gp33 (**a**) or H-2D^b–NP396 (**b**) and then assessed, on days 8, 15 and 30 after infection of recipients with LCMV Armstrong infection, as CD45.2$^+$ (*Atg7*$^{fl/fl}$ or *Atg7*$^{fl/fl}$*Gzmb*-Cre) donor cells or CD45.1$^+$ (C57BL/6) donor cells (middle). Far right, appearance of tetramer-positive T cells (key, donor source) in the peripheral blood of chimeras from day 8 to day 30 after infection, presented relative to that at day 8 after infection, set as 100%. (**c**) Frequency of CD45.2$^+$ antigen-specific CD8$^+$ T cells in the spleen, liver and lungs on day 30 after infection as in **a**,**b**. Data are representative of two independent experiments with three to four mice per group (error bars, s.e.m.).

liquid chromatography–coupled mass-spectrometry metabolomics platform. Among the metabolites that were significantly different in *Atg7*-sufficient cells versus *Atg7*-deficient cells (**Supplementary Table 1**), many were in well-defined metabolic pathways with clear links to cell survival, and some have been linked to T cell differentiation (**Supplementary Fig. 6**). For example, among the pathways that were significantly different in the genotypes were the carnitine shuttle and di-unsaturated fatty acid β-oxidation, both of which are part of fatty acid metabolism in the mitochondria (**Fig. 7a**). T cell–intrinsic mitochondrial fatty acid oxidation (FAO) has been shown to be a critical metabolic pathway for the stable development of long-lived memory T cells[26,27]. These data might indicate that autophagy contributes to the production of the lipid substrates for mitochondrial FAO and the fueling of oxidative phosphorylation in these cells[28]. Consistent with a role for autophagy in lipid metabolism in T cells during the transition to the memory phase, our metabolite analysis showed that lipid biosynthetic pathways were dysregulated in the absence of Atg7 (**Fig. 7a**). Also of note, the glucosamine 6-phosphate and glycan-biosynthesis pathways were perturbed in *Atg7*-deficient T cells (**Fig. 7a** and **Supplementary Fig. 6**). The hexosamine pathway provides substrates for the glycosylation of receptors for growth factor cytokines, which leads to receptor stability and the maintenance of survival signals[29]. Given the importance of growth factor cytokines in supporting the development of memory T cells[2], it is possible that T cells lacking autophagy machinery cannot maintain the proper growth factor signals that support memory T cell development, linking autophagy to glycosylation and the maintenance of cellular metabolism.

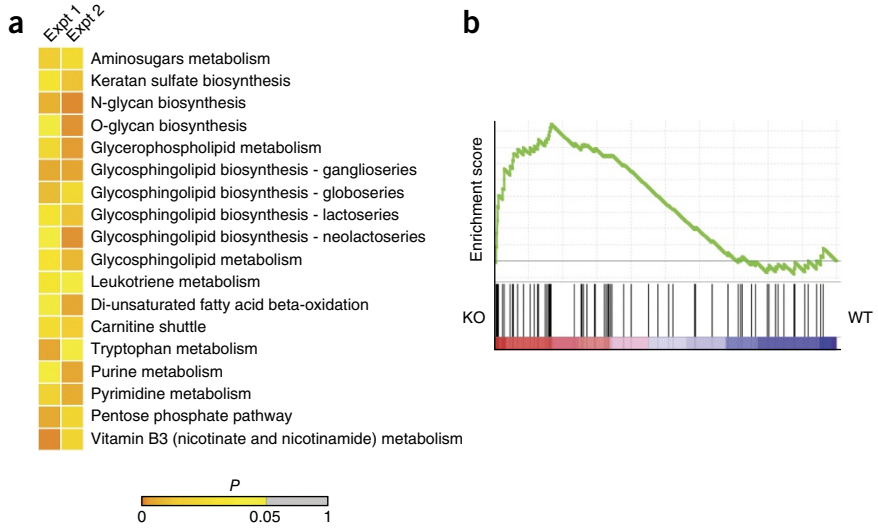

Figure 7 Metabolomic and transcriptomic analysis of *Atg7*-deficient CD8$^+$ T cells. (**a**) Pathways of metabolites regulated differently in H-2D^b–gp33$^+$ CD8$^+$ T cells isolated from *Atg7*$^{fl/fl}$*Gzmb*-Cre mice ($n = 3$) at day 8 after infection with LCMV Armstrong strain, relative to the regulation of these metabolites in their counterparts from *Atg7*$^{fl/fl}$ mice ($n = 3$) treated the same way (columns indicate two independent experiments (Expt 1 and Expt 2)). (**b**) Gene-set–enrichment analysis of genes in T cells associated with the metabolic enzymes underlying the metabolic pathways with the greatest difference in regulation in *Atg7*$^{fl/fl}$*Gzmb*-Cre cells (KO) relative to that in *Atg7*$^{fl/fl}$ cells (WT) in **a**. $P = 0.024$ (calculated by the gene-set-enrichment analysis program). Data are from two independent experiments with samples pooled from three mice per genotype.

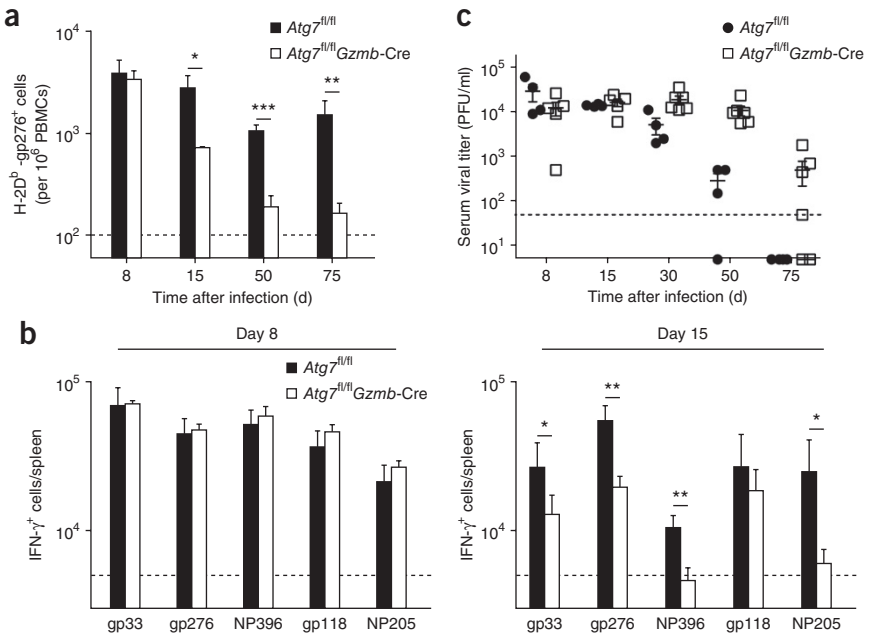

Figure 8 Autophagy in CD8$^+$ T cells is essential for regulating chronic infection with LCMV. (**a**) Kinetics of the appearance of H-2D^b–gp276$^+$ T cells in the peripheral blood of *Atg7*$^{fl/fl}$ and *Atg7*$^{fl/fl}$*Gzmb*-Cre mice at various times (horizontal axis) after infection with LCMV clone 13. (**b**) Total IFN-γ-secreting cells in spleens obtained from mice at day 8 or day 15 after infection as in **a**, assessed after 5 h of stimulation *ex vivo* with various peptides (horizontal axes). (**c**) Viral titers in serum of mice at various times (horizontal axis) after infection as in **a**. Each symbol represents an individual mouse; small horizontal lines indicate the mean (±s.e.m.). $*P \leq 0.05$, $**P \leq 0.005$ and $***P \leq 0.0005$ (unpaired *t*-test). Data are representative of two independent experiments with three to five mice per group (error bars, s.e.m.).

We further confirmed the metabolomics data reported above by assessing the expression of genes encoding the enzymes associated those metabolite activities. By gene-set–enrichment analysis[30] with the genes encoding those enzymes as a gene set, we found that the expression of genes encoding molecules involved in those metabolic activities was clearly associated with the *Atg7*-deficient genotype (**Fig. 7b**). Overall, several metabolic pathways were altered in *Atg7*-deficient T cells at day 8 after infection, a result that, when integrated with our transcriptomic studies, suggested that autophagy supports metabolic homeostasis in CD8$^+$ T cells during the transition to the memory phase.

Autophagy in CD8$^+$ T cells is essential for viral control

Autophagy was required for the formation of memory CD8$^+$ T cells during an acute viral infection, as shown above. Next we determined whether autophagy regulates CD8$^+$ T cell responses during a chronic viral infection. We challenged *Atg7*$^{fl/fl}$*Gzmb*-Cre mice with the LCMV strain clone 13, which causes chronic infection[31]. During chronic infection, antigen-specific T cells gradually diminish in their effector functionality and become exhausted cells due to prolonged persistence of antigen in the host[32]. During chronic infection, antigen-specific CD8$^+$ T cells in *Atg7*$^{fl/fl}$*Gzmb*-Cre mice again mounted an initial response to the virus in the peripheral blood, as well as in lymphoid and nonlymphoid tissues at day 8 after infection, similar to *Atg7*$^{fl/fl}$ mice (**Fig. 8a** and **Supplementary Fig. 7a**,**b**). *Ex vivo* stimulation of splenocytes at day 8 after infection showed little difference in the number of cells producing IFN-γ (**Fig. 8b**). However, by day 15 after infection, most LCMV-specific T cells were lost in *Atg7*$^{fl/fl}$*Gzmb*-Cre mice throughout lymphoid and nonlymphoid tissues, similar to results obtained for the acute infection model (**Fig. 8a** and **Supplementary Fig. 7c**,**d**). The reduction observed was also reflected in the number of IFN-γ-producing cells after stimulation *ex vivo* (**Fig. 8b**). As a consequence of the loss of most antigen-specific cells, viral control was compromised in *Atg7*$^{fl/fl}$*Gzmb*-Cre mice (**Fig. 8c**). These data further indicated a considerable survival defect in the *Atg7*-deficient LCMV-specific effector CD8$^+$ T cells: not only were these cells compromised in memory CD8$^+$ T cell differentiation, they also failed to survive in the chronic infection model.

DISCUSSION

Our finding that proliferating T cells underwent decreased autophagy *in vivo* was unexepected, because published *in vitro* studies have shown that autophagy is increased in T cells after TCR stimulation[9,12,13]. Discrepancies between our study and those published studies might be explained by the vastly different conditions of TCR stimulation *in vivo* versus *in vitro*. In addition, in some of those published studies, only a single aspect of the autophagy pathway, such as the number of autophagosomes or the amount of lipidated LC3b-II, was used to assess autophagy activity in cultured T cells. As the autophagy pathway can be blocked at any point along its progression, it has become clear that measuring a single component in the pathway, rather than measuring flux through the pathway (as done here), is not reflective of whether autophagy is activated or blocked[7]. In contrast, the autophagic flux assays used in our experiments meet the current standards; thus, we propose a distinct model of the kinetics of *in vivo* autophagy activity in antigen-specific CD8$^+$ T cells after viral infection.

Our findings on the kinetics of autophagy *in vivo* were consistent with our results in which genes encoding molecules essential for autophagy were deleted from antigen-specific CD8$^+$ T cells. The *in vivo* kinetics of autophagy indicated that activated T cells were able to proliferate with very low autophagy activity; indeed both autophagy-deficient and wild-type virus-specific CD8$^+$ T cell populations were able to expand similarly in most tissues. However, that similar expansion of antigen-specific CD8$^+$ T cell populations in mice with null mutation of autophagy molecule–encoding genes and wild-type mice was unexpected, because a published study has shown that deletion of genes encoding autophagy-related molecules results in compromised T cell proliferation after *in vitro* stimulation via the TCR[9]. The T cells used in that published study were defective in autophagy for long periods of time before being assayed because the genes encoding autophagy-related molecules were deleted during T cell development[9]. It is known that T cells deficient in the genes encoding autophagy-related molecules are transcriptionally and phenotypically distinct from wild-type T cells[9,10,15,33]. To avoid this complication in our studies, we deleted the genes encoding autophagy-related molecules specifically from cells expressing granzyme B after T cell activation; therefore, naive T cells were normal at the time of viral infection. Thus, robust expansion of CD8$^+$ T cell populations in the absence of genes encoding autophagy-related molecules would

suggest that activated T cells can proliferate and differentiate into effector cells without autophagy, which is consistent with the *in vivo* kinetics of autophagy in antigen-specific CD8$^+$ T cells.

In contrast to results obtained for the T cell clonal-expansion phase, autophagy was required for the survival of effector T cells that then formed memory T cells during the contraction phase, when effector T cells undergo substantial changes. In this phase, effector T cells, having just finished many rounds of vigorous cell divisions, potentially accumulate protein aggregates, reactive oxygen species and other superfluous cellular content[34–38]. Autophagy could serve various prosurvival functions in these cells, including the removal of damaged mitochondria that generate reactive oxygen species or misfolded proteins[39,40]. Thus, upregulation of autophagy in virus-specific CD8$^+$ T cells upon the conclusion of clonal expansion is important during the contraction phase.

Our results have implications for published studies linking the major regulator of autophagy mTOR to the differentiation of memory CD8$^+$ T cells[27,41]. Such studies have demonstrated that inhibition of mTOR by rapamycin improves not only the magnitude of memory CD8$^+$ T cells but also their quality[27,41]. These effects of rapamycin on antigen-specific CD8$^+$ T cells might result from increased autophagy during the expansion and contraction phases. Active mTOR signaling directly downregulated autophagy and therefore inhibition of mTOR would probably enhance autophagy activity[42]. Thus, future studies should investigate whether treatment with rapamycin upregulates autophagy in antigen-specific CD8$^+$ T cells and whether increased autophagy improves the differentiation of memory CD8$^+$ T cells.

Our metabolomics analysis provided insight into regulation of the metabolic pathway by autophagy in virus-specific CD8$^+$ T cells. The unbiased metabolite data revealed that mitochondrial FAO, which has been shown to be critical for the generation of memory T cells[26,27], was dysregulated in *Atg7*-deficient T cells at the peak of clonal expansion, when antigen-specific T cells transition to the memory phase. A study of metabolomic profiles in a mouse cancer model has reported that *Atg7*-deficient tumor cells have defective mitochondria and diminished FAO[43]. We speculate that T cell–intrinsic autophagy may be important for the generation of lipid substrates for mitochondrial FAO, consistent with published studies showing that autophagy can regulate lipid metabolism via the breakdown of cellular lipid stores[44]. Precisely how the substrates for mitochondrial FAO are used or generated by memory T cells, and whether autophagy directly regulates mitochondrial FAO in antigen-specific effector CD8$^+$ T cells, are subjects for future work.

In addition to showing the importance of autophagy during an acute viral infection, our data demonstrated that autophagy in virus-specific CD8$^+$ T cells was essential for cell survival and for viral control during a chronic infection. It is well established that activated CD8$^+$ T cells during chronic infections or in tumor environments differentiate into exhausted T cells. The 'rejuvenation' of exhausted T cells is a promising approach for treating chronic infections and cancer. Thus, our data suggest critical role for autophagy in the formation and survival of exhausted CD8$^+$ T cells that can be targeted for immunotherapy.

In summary, our data have established that the autophagy pathway is dynamically regulated throughout the CD8$^+$ T cell response and is critical for the formation of T cell memory. Autophagy seems to have a role in the metabolic homeostasis of effector CD8$^+$ T cells during their transition into memory cells. Our studies have implications for the development of effective vaccination strategies and anticancer immunotherapy through targeting of the autophagy pathway and/or other metabolic pathways.

METHODS

Methods and any associated references are available in the online version of the paper.

Accession codes. GEO: microarray data, GSE57047.

Note: Any Supplementary Information and Source Data files are available in the online version of the paper.

ACKNOWLEDGMENTS

We thank A. Rao (La Jolla Institute for Allergy and Immunology) for the MSCV-IRES-Thy-1.1 retroviral vector; J. Jacob (Emory University) for *Gzmb*-Cre transgenic mice; V. Tran for the LC-MS experiments; R. Karaffa and S. Durham for sorting cells by flow cytometry at the Emory Flow Cytometry Core Facility; and A. Rae for assistance in the use of ImageStream. Supported by the US National Institutes of Health (R01 AI030048 to R.A. and R01 AI084887 to H.W.V.), the Mérieux Foundation (R.A.) and the Crohn's and Colitis Foundation (H.W.V.).

AUTHOR CONTRIBUTIONS

X.X., K.A., S.L., M.W.B., J.M., D.R.G., D.P.J., H.W.V. and R.A. designed the research; X.X., K.A., S.L., J.-H.H., L.Y., W.G.T. and B.T.K. performed experiments. X.X., K.A., S.L., M.W.B., E.L.P., D.R.G., D.P.J., H.W.V. and R.A. analyzed data; and X.X., K.A., S.L., E.L.P., H.W.V. and R.A. wrote the manuscript.

COMPETING FINANCIAL INTERESTS

The authors declare no competing financial interests.

1. Williams, M.A. & Bevan, M.J. Effector and memory CTL differentiation. *Annu. Rev. Immunol.* **25**, 171–192 (2007).
2. Kaech, S.M. & Wherry, E.J. Heterogeneity and cell-fate decisions in effector and memory CD8+ T cell differentiation during viral infection. *Immunity* **27**, 393–405 (2007).
3. Kaech, S.M. *et al.* Selective expression of the interleukin 7 receptor identifies effector CD8 T cells that give rise to long-lived memory cells. *Nat. Immunol.* **4**, 1191–1198 (2003).
4. Sarkar, S. *et al.* Functional and genomic profiling of effector CD8 T cell subsets with distinct memory fates. *J. Exp. Med.* **205**, 625–640 (2008).
5. Joshi, N.S. *et al.* Inflammation directs memory precursor and short-lived effector CD8+ T cell fates via the graded expression of T-bet transcription factor. *Immunity* **27**, 281–295 (2007).
6. Levine, B., Mizushima, N. & Virgin, H.W. Autophagy in immunity and inflammation. *Nature* **469**, 323–335 (2011).
7. Mizushima, N., Yoshimori, T. & Levine, B. Methods in mammalian autophagy research. *Cell* **140**, 313–326 (2010).
8. Walsh, C.M. & Edinger, A.L. The complex interplay between autophagy, apoptosis, and necrotic signals promotes T-cell homeostasis. *Immunol. Rev.* **236**, 95–109 (2010).
9. Pua, H.H., Dzhagalov, I., Chuck, M., Mizushima, N. & He, Y.W. A critical role for the autophagy gene Atg5 in T cell survival and proliferation. *J. Exp. Med.* **204**, 25–31 (2007).
10. Stephenson, L.M. *et al.* Identification of Atg5-dependent transcriptional changes and increases in mitochondrial mass in Atg5-deficient T lymphocytes. *Autophagy* **5**, 625–635 (2009).
11. Wang, R.C. & Levine, B. Autophagy in cellular growth control. *FEBS Lett.* **584**, 1417–1426 (2010).
12. Hubbard, V.M. *et al.* Macroautophagy regulates energy metabolism during effector T cell activation. *J. Immunol.* **185**, 7349–7357 (2010).
13. Li, C. *et al.* Autophagy is induced in CD4+ T cells and important for the growth factor-withdrawal cell death. *J. Immunol.* **177**, 5163–5168 (2006).
14. Rubinsztein, D.C., Codogno, P. & Levine, B. Autophagy modulation as a potential therapeutic target for diverse diseases. *Nat. Rev. Drug Discov.* **11**, 709–730 (2012).
15. Pua, H.H., Guo, J., Komatsu, M. & He, Y.W. Autophagy is essential for mitochondrial clearance in mature T lymphocytes. *J. Immunol.* **182**, 4046–4055 (2009).
16. Pankiv, S. *et al.* p62/SQSTM1 binds directly to Atg8/LC3 to facilitate degradation of ubiquitinated protein aggregates by autophagy. *J. Biol. Chem.* **282**, 24131–24145 (2007).
17. Shvets, E., Fass, E. & Elazar, Z. Utilizing flow cytometry to monitor autophagy in living mammalian cells. *Autophagy* **4**, 621–628 (2008).
18. Gump, J.M. *et al.* Autophagy variation within a cell population determines cell fate through selective degradation of Fap-1. *Nat. Cell Biol.* **16**, 47–54 (2014).
19. Kimura, S., Noda, T. & Yoshimori, T. Dissection of the autophagosome maturation process by a novel reporter protein, tandem fluorescent-tagged LC3. *Autophagy* **3**, 452–460 (2007).
20. Kuma, A. *et al.* The role of autophagy during the early neonatal starvation period. *Nature* **432**, 1032–1036 (2004).

21. Hara, T. *et al.* Suppression of basal autophagy in neural cells causes neurodegenerative disease in mice. *Nature* **441**, 885–889 (2006).
22. Jacob, J. & Baltimore, D. Modelling T-cell memory by genetic marking of memory T cells *in vivo*. *Nature* **399**, 593–597 (1999).
23. Masopust, D., Murali-Krishna, K. & Ahmed, R. Quantitating the magnitude of the lymphocytic choriomeningitis virus-specific CD8 T-cell response: it is even bigger than we thought. *J. Virol.* **81**, 2002–2011 (2007).
24. Waggoner, S.N., Cornberg, M., Selin, L.K. & Welsh, R.M. Natural killer cells act as rheostats modulating antiviral T cells. *Nature* **481**, 394–398 (2012).
25. Lang, P.A. *et al.* Natural killer cell activation enhances immune pathology and promotes chronic infection by limiting CD8$^+$ T-cell immunity. *Proc. Natl. Acad. Sci. USA* **109**, 1210–1215 (2012).
26. van der Windt, G.J. *et al.* Mitochondrial respiratory capacity is a critical regulator of CD8$^+$ T cell memory development. *Immunity* **36**, 68–78 (2012).
27. Pearce, E.L. *et al.* Enhancing CD8 T-cell memory by modulating fatty acid metabolism. *Nature* **460**, 103–107 (2009).
28. O'Sullivan, D. *et al.* Memory CD8$^+$ T cells use cell-intrinsic lipolysis to support the metabolic programming necessary for development. *Immunity* **41**, 75–88 (2014).
29. Wellen, K.E. *et al.* The hexosamine biosynthetic pathway couples growth factor-induced glutamine uptake to glucose metabolism. *Genes Dev.* **24**, 2784–2799 (2010).
30. Subramanian, A. *et al.* Gene set enrichment analysis: a knowledge-based approach for interpreting genome-wide expression profiles. *Proc. Natl. Acad. Sci. USA* **102**, 15545–15550 (2005).
31. Wherry, E.J., Blattman, J.N., Murali-Krishna, K., van der Most, R. & Ahmed, R. Viral persistence alters CD8 T-cell immunodominance and tissue distribution and results in distinct stages of functional impairment. *J. Virol.* **77**, 4911–4927 (2003).
32. Zajac, A.J. *et al.* Viral immune evasion due to persistence of activated T cells without effector function. *J. Exp. Med.* **188**, 2205–2213 (1998).
33. Jia, W., Pua, H.H., Li, Q.J. & He, Y.W. Autophagy regulates endoplasmic reticulum homeostasis and calcium mobilization in T lymphocytes. *J. Immunol.* **186**, 1564–1574 (2011).
34. Kaech, S.M., Hemby, S., Kersh, E. & Ahmed, R. Molecular and functional profiling of memory CD8 T cell differentiation. *Cell* **111**, 837–851 (2002).
35. Rathmell, J.C., Farkash, E.A., Gao, W. & Thompson, C.B. IL-7 enhances the survival and maintains the size of naive T cells. *J. Immunol.* **167**, 6869–6876 (2001).
36. Ma, A., Koka, R. & Burkett, P. Diverse functions of IL-2, IL-15, and IL-7 in lymphoid homeostasis. *Annu. Rev. Immunol.* **24**, 657–679 (2006).
37. Jones, R.G. & Thompson, C.B. Revving the engine: signal transduction fuels T cell activation. *Immunity* **27**, 173–178 (2007).
38. Grayson, J.M., Laniewski, N.G., Lanier, J.G. & Ahmed, R. Mitochondrial potential and reactive oxygen intermediates in antigen-specific CD8$^+$ T cells during viral infection. *J. Immunol.* **170**, 4745–4751 (2003).
39. Paul, S., Kashyap, A.K., Jia, W., He, Y.W. & Schaefer, B.C. Selective autophagy of the adaptor protein Bcl10 modulates T cell receptor activation of NF-κB. *Immunity* **36**, 947–958 (2012).
40. Komatsu, M. *et al.* The selective autophagy substrate p62 activates the stress responsive transcription factor Nrf2 through inactivation of Keap1. *Nat. Cell Biol.* **12**, 213–223 (2010).
41. Araki, K. *et al.* mTOR regulates memory CD8 T-cell differentiation. *Nature* **460**, 108–112 (2009).
42. Kim, J., Kundu, M., Viollet, B. & Guan, K.L. AMPK and mTOR regulate autophagy through direct phosphorylation of Ulk1. *Nat. Cell Biol.* **13**, 132–141 (2011).
43. Guo, J.Y. *et al.* Autophagy suppresses progression of K-ras-induced lung tumors to oncocytomas and maintains lipid homeostasis. *Genes Dev.* **27**, 1447–1461 (2013).
44. Singh, R. *et al.* Autophagy regulates lipid metabolism. *Nature* **458**, 1131–1135 (2009).

ONLINE METHODS

Mice and infection. *Atg7*$^{fl/fl}$ mice and *Atg5*$^{fl/fl}$ mice were generated and characterized as described[20,21]. Mice with conditional null mutation were generated by crossing of *Atg7*$^{fl/fl}$ mice and *Atg5*$^{fl/fl}$ mice to *Gzmb*-Cre mice[22]. To generate P14 chimeric mice bearing LCMV-specific CD8$^+$ T cells, P14 (CD45.1$^+$ or Thy-1.1$^+$) cells with an engineered TCR that recognizes the H-2D^b–gp33 epitope were adoptively transferred intravenously (1×10^4 antigen-specific CD8$^+$ T cells per mouse) into wild-type C57BL/6 mice (The Jackson Laboratory). For acute infection, mice were infected by intraperitoneal injection of 2×10^5 plaque-forming unit (PFU) of the Armstrong strain of LCMV. For chronic infection, mice were infected by intravenous injection of 2×10^6 PFU of the clone 13 strain of LCMV. All animal experiments were approved by the Institutional Animal Care and Use Committee of Emory University.

Retroviral transduction. Overexpression of transgenes in P14 cells was achieved with the MSCV-IRES-Thy-1.1 retroviral vector (17442; Addgene), provided by A. Rao. The gene encoding LC3b was cloned from mouse cDNA and then was fused at the amino terminus to sequence encoding Emerald GFP (Invitrogen). The G120A mutant was made with the Quickchange kit (Agilent Technology). For mCherry constructs, the gene encoding mCherry (Clontech Laboratories) was fused to the amino terminus of sequence encoding GFP-tagged wild-type Lc3b or its G120A mutant. For the activation of P14 cells, gp33 peptide (200 μg) was injected intravenously into P14 (CD45.1$^+$Thy-1.1$^-$) mice. Splenocytes were then isolated 18–24 h after injection of gp33 peptide and were 'spin transduced' with the desired retrovirus. We adoptively transferred 1×10^4 retroviral transduced P14 cells into naive C57BL/6 mice, which we immediately infected intraperitoneally with 2×10^5 PFU LCMV Armstrong strain. Retroviral transduction of hematopoietic stem cells was carried out as described[45]. The transduced cells were adoptively transferred into lethally irradiated mice.

Flow cytometry and antibodies. The following antibodies were from BD Bioscience: anti-CD8 (53-6.7), anti-Thy-1.1 (OX-7), anti-CD45.1 (A20), anti-CD45.2 (104), anti-CD44 (IM7), anti-IFN-γ (XMG1.2) and anti-TNF (MP6-XT22). A BrdU flow kit (559619; BD Bioscience) was used for staining with BrdU (5-bromodeoxyuridine). Anti-KLRG1 (2F1) was from Southern Biotech. Anti-CD127 (A7R34) and CD62L (MEL-14) were from eBioscience. Major histocompatibility comples class I tetramers were prepared as described[46]. All the analyses were done on a FACSCanto II or LSR II flow cytometer (BD Biosciences).

Cellular imaging. Cells were analyzed on an ImageStream Mark II (Amnis) with INSPIRE software. Images were acquired at a magnification of ×60 or ×40 with a low-speed and high-sensitivity setting. Single focused cells were selected for image collection. Data were analyzed with IDEA software. Spot-counting analysis was used for evaluation of LC3b puncta–positive cells in each sample.

Quantitative PCR. For analysis of genomic deletion of *Atg7*^{fl}, H-2D^b–gp33–specific CD8$^+$ T cells were sorted and DNA was extracted with a DNeasy kit (Qiagen). Quantitative PCR was carried out with iQSYBR Green Supermix (BioRad) and primers flanking one *lox*P-flanked site (forward, 5′-AGCTTGGCTGCTACTTCTGC-3′; reverse, 5′-TGCAGGACAGAGACCATCAG-3′) and primers targeting the allele encoding PD-1 as a loading control (forward, 5′-GAGGTCCTTTCACTCTCCACG-3′; reverse, 5′-CGACTTGTGTGCATGCATAGTACC-3′). Primers used to quantify mRNA were as follows: LC3b-encoding mRNA, 5′-CACTGCTC TGTCTTGTGTAGGTTG-3′ (forward) and 5′-TCGTTGTGCCTTTATTAG TGCATC-3′ (reverse); and p62-encoding mRNA, 5′-AGCTGCCCTCAG CCCTCTA-3′ (forward) and 5′-GGCTTCTCTTCCCTCCATGTT-3′ (reverse). 18s rRNA was used as internal control for qRT-PCR: 5′-GTAACCCGT TGAACCCCATT-3′ (forward) and 5′-CCATCCAATCGGTAGTAGCCG-3′ (reverse).

Cell sorting. Total activated CD8$^+$ T cells on day 8 after infection with LCMV were stained with anti-CD8, anti-CD44 and anti-CD62L (identified above) and were sorted with a FACSAria II (BD). H-2D^b–gp33-specific cells were stained with anti-CD8, anti-CD44 and anti-TCR (identified above) through the use of the H-2D^b–gp33 tetramer[46]. The typical purity after cell sorting was between 95% and 99%.

Immunoblot analysis. Whole-cell lysates of cell populations were resolved by 4–15% SDS-PAGE and then were transferred to a PVDF (polyvinylidene diuoride) membrane (Millipore). The membrane was probed with rabbit anti-β-actin (13E5; Cell Signaling Technology), rabbit anti-Atg7 (A2856; Sigma-Aldrich), mouse anti-Atg5 (7C6; NanoTools), rabbit anti-LC3 (L7543; Sigma-Aldrich) or guinea pig anti-p62 (GP62-C (Progen Biotechnik) and P0067 (Sigma-Aldrich)); secondary horseradish peroxidase–linked antibodies were goat anti-rabbit (7074; Cell Signaling Technology), goat anti-mouse (1034-05; Southern Biotech) and goat anti-guinea pig (106-035-003; Jackson ImmunoResearch). The blots were developed in LumiGLO reagent (Cell Signaling Technology) before exposure to X-ray films (Kodak).

Generation of bone marrow chimeras. Bone marrow was collected from *Atg7*$^{fl/fl}$ (CD45.2$^+$) mice, *Atg7*$^{fl/fl}$*Gzmb*-Cre (CD45.2$^+$) mice or wild-type C57BL/6 (CD45.1$^+$) mice. For each chimera, 20×10^6 cells of 1:1 mixture of *Atg7*$^{fl/fl}$ (or *Atg7*$^{fl/fl}$*Gzmb*-Cre) and C57BL/6 bone marrow cells were transferred intravenously into lethally irradiated (two doses of 550 rads) wild-type C57BL/6 (CD45.1$^+$) recipients. Recipient mice were allowed 8–10 weeks for reconstitution before infection with LCMV Armstrong strain.

Liquid chromatography–mass spectrometry metabolomic analysis. The metabolomics analysis was performed as described[48]. Cell extracts were treated with acetonitrile (2:1, v/v) and were centrifuged at 14,000*g* for 5 min at 4 °C for removal of proteins. Samples were maintained at 4 °C in an autosampler until injection. An Orbitrap Velos mass spectrometer (Thermo Fisher Scientific) coupled with switching dual chromatography (an anion-exchange column and a C18 reverse-phase column) was used for data collection, via positive-ion electrospray ionization. Each sample was run with three to six analytical replicates, depending on available source material. Mouse naive CD8$^+$ T cells, kidney and splenocyte tissues were also run as analytical controls. Metabolite features were extracted and quantified with apLCMS software (version 5.9.8)[47]. Only features that were detected in 12 or more injection samples (including analytical replicates) were retained for further analysis. This filtering led to 3,270 metabolite features from the anion-exchange column and 6,300 from the C18 column. Data were $\log_2$ transformed, averaged among analytical replicates, and normalized by total ion intensity. Missing values were imputed with half mean of the feature in all detected samples. Student's *t*-test was used for comparison of null-mutation and wild-type groups. Metabolic-pathway analysis was performed by mummichog software 0.9.6 with default parameters[48]. The top 500 metabolite features in the *t*-test were used as input to mummichog, and the total list of features were used as reference. The mummichog software tested the enrichment of input metabolites against random data resampled from the reference list and produced an empirical *P* value per pathway[48]. Input metabolites in the significant pathways ($P < 0.05$ in both experiments) were linked in a network figure by known metabolic reactions (**Supplementary Fig. 6**).

Microarray analysis. H-2D^b–gp33-specific CD8$^+$ T cells from mice at day 8 after acute LCMV infection were sorted by flow cytometry on the basis of CD8 expression and tetramer staining. RNA was isolated with an RNeasy kit according to the manufacturer's protocol (Qiagen). RNA was amplified, biotinylated and hydridized on mouse 430.2 Affymetrix microarray chips at the Microarray Core (Dana Farber Cancer Institute). The expression of metabolic enzymes underlying the data in **Supplementary Figure 6** was assessed for association with the null mutation or wild-type genotype. All 'enzyme commission' numbers in the reactions in **Supplementary Figure 6** were cross-referenced with the mouse genome for the genes encoding them. Only genes expressed in T cells were included for this analysis. Positive expression in T cells was according to the definition of the Immunological Genome Project as signal intensity higher than 128 units in any of their microarray files (a total of 89 microarrays of T cell populations, retrieved on 22 February 2014 from the database of the Immunological Genome Project). The resulting genes (*Gpd1l*, *Kdsr*, *Ado*, *Acox1*, *Gmpr2*, *Tkt*, *Alg5*, *Alg13*, *Hprt*, *Nampt*, *Gsta4*, *Gstk1*, *Gstm1*, *Gstm4*, *Gsto1*, *Gstp1*, *Gstp2*, *Gstt2*, *Hpgds*, *Gfpt1*, *Adk*, *Nagk*,

doi:10.1038/ni.3025

Dck, *Sphk1*, *Sphk2*, *Prps1*, *Prps2*, *Cept1*, *Ept1*, *Cdipt*, *Plb1*, *Acot2*, *Lpin1*, *Lpin2*, *Pde1b*, *Pde2a*, *Pde3b*, *Pde4a*, *Pde4d*, *Pde7a*, *Pde8a*, *Pde5a*, *Arsa*, *Gba2*, *Galc*, *Bst1*, *Cd38*, *Asah1*, *Asah2*, *Ada*, *Ampd1*, *Ampd2*, *Ampd3*, *Cant1*, *Enpp1*, *Itpa*, *Enpp4*, *Aldoa*, *Aldoc*, *Sgpl1*, *Npl*, *Acsl1*, *Acsl3*, *Acsl4* and *Acsl5*) were used as a custom gene set in a gene matrix–transposed file and were tested in the Gene Set Enrichment Analysis program[30]. The 'preranked' method of this program was used, in which the genes were ranked by *t*-statistic between samples from mice with a null mutation and those from wild-type mice.

Statistical analysis. Statistics were analyzed with GraphPad Prism 5 software. *P* values were calculated on the basis of a two-tailed unpaired Student's *t*-test, with the assumption of normal distribution of data and equal sample variance. Sample size was not predetermined via statistical means, but the number of mice used in the study was consistent with published work of similar nature. All mice used for the study were included for a robust statistical analysis, with no randomization or blinding involved.

45. Jordan, M.S. Genetic reconstitution of bone marrow for the study of signal transduction *ex vivo*. *Methods Mol. Biol.* **332**, 331–342 (2006).
46. Murali-Krishna, K. *et al.* Counting antigen-specific CD8 T cells: a reevaluation of bystander activation during viral infection. *Immunity* **8**, 177–187 (1998).
47. Yu, T., Park, Y., Johnson, J.M. & Jones, D.P. apLCMS–adaptive processing of high-resolution LC/MS data. *Bioinformatics* **25**, 1930–1936 (2009).
48. Li, S. *et al.* Predicting network activity from high throughput metabolomics. *PLoS Comput. Biol.* **9**, e1003123 (2013).